ADVANCED MATERIALS

DOI: 10.1002/adma.200700883

Lithiated MoO_3 Nanobelts with Greatly Improved Performance for Lithium Batteries**

By *Liqiang Mai, Bin Hu, Wen Chen,* Yanyuan Qi, Changshi Lao, Rusen Yang, Ying Dai,* and *Zhong Lin Wang**

Recently, nanostructured materials have attracted great interest in the field of lithium-ion batteries, essentially because of their substantial advantages, such as short transport path lengths for both electrons and Li^+ ions, a large amount of contact surface area between the electrode and electrolyte, and large flexibility and toughness for accommodating strain introduced by Li^+ insertion/extraction.[1–3] Among the transition-metal oxides, nanostructured MoO_3 has been extensively investigated as a key material for fundamental research and technological applications in optical devices, smart windows, catalysts, sensors, lubricants, and electrochemical storage.[4–7] There are two basic polytypes of MoO_3: orthorhombic MoO_3 (α-type) being a thermodynamically stable phase, and the metastable monoclinic MoO_3 (β-type) with a ReO_3-type structure. The most important structural characteristic of α-MoO_3 is its structural anisotropy, which can be considered as a layered structure parallel to (010) (See the inset of Fig. S1, Supporting Information). Each layer is composed of two sub-layers, each of which is formed by corner-sharing octahedra along [001] and [100]; the two sub-layers stack together by sharing the edges of the octahedra along [001]. An alternate stack of these layered sheets along [010] would lead to the formation of α-MoO_3, where a van der Waals interaction would be the major binding force between the piled sheets. One might take advantage of the intrinsic structural anisotropy of α-MoO_3 for tuning its properties by interlayer structural modification, annealing, and lithiation.[5,8,9] In this Communication, we report the electroactivity of α-MoO_3 nanobelts after lithiation that show superior performance to non-lithiated α-MoO_3 nanobelts.

An X-ray diffraction (XRD) measurement was performed using a D/MAX-III X-ray diffractometer. Fourier-transformed infrared (FTIR) absorption spectra were recorded using the 60-SXB IR spectrometer. Raman spectra were taken using a Renishaw RM-1000 laser Raman microscopy system. Scanning electron microscopy (SEM) images were collected with a JSM-5610 and FES-EM LEO 1530. Transmission electron microscopy (TEM), high-resolution transmission electron microscopy (HRTEM), and selected-area electron diffraction (SAED) were recorded by using a JEOL JEM-2010 FEF microscope. The electrochemical properties were studied with a multichannel battery testing system. Batteries were fabricated using a lithium pellet as the negative electrode; 1 M $_6$ in ethylene carbon (EC)/dimethyl carbonate (DMC) as the electrolyte; and a pellet made of the nanobelts, acetylene black and PTFE in a 10:7:1 ratio as the positive electrode. The fabrication of a single nanobelt-based device has been described in detail elsewhere.[10]

XRD measurement was first used to study the phase and lattice modification of the nanobelts before and after lithiation (Fig. 1A). The diffraction peaks of the XRD pattern for both samples can be readily indexed to be orthorhombic with lattice constants of $a = 3.962$ Å, $b = 13.85$ Å, $c = 3.697$ Å (International Centre for Diffraction Data (ICDD) No. 05-0508). No peaks of any other phases were detected, indicating the high purity of the MoO_3 nanobelts. For the non-lithiated MoO_3 nanobelts, the stronger intensities of (020), (040), and (060) peaks than those for the bulk MoO_3 (Fig. S1, Supporting Information) indicates the anisotropic growth of the nanostructure as well as the preferred orientation of the nanobelts on the substrate. Importantly, in comparison to the non-lithiated sample, there is a small shift of the (020) peak toward a lower diffraction angle for the lithiated sample. This is direct evidence of an expanded *b*-plane interlayer distance for 0.065 Å after lithiation, possibly due to the introduction of Li interstitials between the layers.

The morphology and microstructure of the products were observed by using SEM and TEM. Before lithiation (Fig. 1B),

[*] Prof. W. Chen, Dr. L. Q. Mai, B. Hu, Y. Y. Qi, Prof. Y. Dai
State Key Laboratory of Advanced Technology for Materials Synthesis and Processing
Institute of Materials Science and Engineering
Wuhan University of Technology
Wuhan, 430070 (P.R. China)
E-mail: chenw@whut.edu.cn
Prof. Z. L. Wang, Dr. L.Q. Mai, C.S. Lao, R.S. Yang
School of Materials Science and Engineering
Georgia Institute of Technology
Atlanta, Georgia 30332-0245 (USA)
E-mail: zhong.wang@mse.gatech.edu

[**] This work was supported by the National Nature Science Foundation of China (50702039, 50672071, 50672072), the Key Project of Chinese Ministry of Education (104207, 105124), the Program for Changjiang Scholars and Innovative Research Team in University (PCSIRT, No. IRT0547), the Ministry of Education, China, the Foundation for Innovation Research Team (2005ABC004), and the Natural Science Foundation (2006ABA310) of Hubei Province, the Wuhan Youth Chenguang Project (20065004116-17). This project is partly supported by National Center for Nanoscience and Technology, China. C.S.L. and Z.L.W. are thankful for support from the US NSF, DARPA, and NIH (CCNE). Supporting Information is available online from Wiley InterScience or from the author

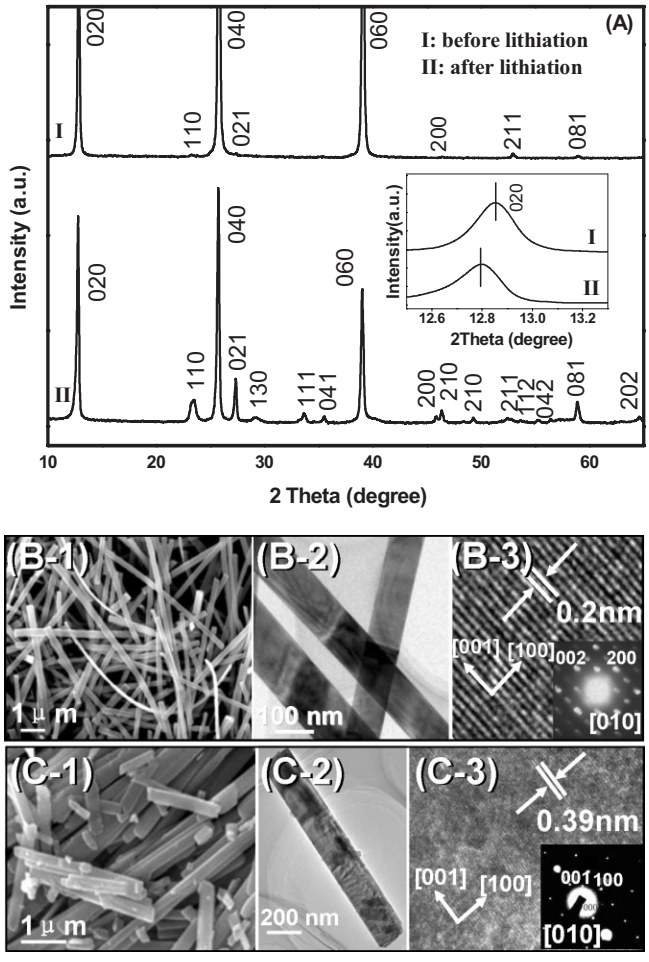

Figure 1. (A) XRD patterns of MoO_3 nanobelts before and after lithiation. The inset is the corresponding (020) diffraction peak. (B, C) SEM, TEM and HRTEM characterization of the nanobelts before and after lithiation, respectively. The insets in the HRTEM images are the corresponding SAED patterns.

the sample showed a long, beltlike morphology with widths of 80–400 nm and lengths of 5–10 μm, and a rectanglelike cross section was clearly visible. For the lithiated sample (Fig. 1C), however, the nanobelt length decreased to 2–6 μm, and some ruptured short segments with lengths of 200–400 nm can clearly be seen in Figure 1C-1. In Figure 1C-2, the surface of the lithiated nanobelt is rougher than that of the non-lithiated sample, with the presence of surface nanoflakes. An SAED pattern (the inset in Fig. 1B-3) recorded with the incident electron beam perpendicular to the nanobelt shows the [010] pattern of α-MoO_3, and the growth direction is [001], the top/bottom surfaces being (010) and the side surfaces being (100). The formation of the dominant (010) surfaces is the result of the anisotropic structure.[11] In α-MoO_3, because of the layered structure along the *b*-axis, the bonding within the layer is dominated by ionic bonding, while the interlayer bonding is dominated by van der Waals forces. Growth along the *c*-axis results in the exposed top and bottom surfaces of the nanobelt being the compacted layers of the MoO_6 octahedra, which have the lowest energy (see the inset model in Fig. S1).

Raman and FTIR spectroscopy were applied to investigate the change in bonding related to MoO_3 nanobelts before and after lithiation. Figure 2A shows the Raman spectra of non-lithiated and lithiated MoO_3 nanobelts. The Raman spectrum of MoO_3 can be discussed in terms of internal and external modes.[12] The highest stretching frequency at 993 cm^{-1} (the so-called molybdyl mode) is attributed to the shortest Mo–O bond, whereas the next highest stretching frequency at 817 cm^{-1} is assigned to the intermediate bridging O–Mo–O bond. The bending modes are located in the medium frequency range, whereas the external modes appear at below 200 cm^{-1}. The Raman data show that intercalation of Li has no significant effect on the structure of the MoO_3 nanobelts. The FTIR spectra in Figure 2B support a consistent conclusion. The stretching mode of Mo-terminal oxygen is located at 999 cm^{-1}. The absorption bands at 867 and 555 cm^{-1} are assigned to stretching vibrations of the O(3) and O(2) atoms linked to two or three molybdenum atoms, respectively.[13,14] The FTIR results confirm that the intercalation of Li has no appreciable influence on the bond vibration and structure of the MoO_3 nanobelts.

The lithiation results in a drastic improvement in the charge-storage capacity and stability of the nanobelts. Figure 3A shows the potential versus capacity curve of the first cycles for the non-lithiated and lithiated MoO_3 nanobelts. The first discharge capacities are 301 and 240 mAh g^{-1} before and after lithiation, respectively, both of which are higher than that for bulk MoO_3 measured under the same conditions. This is likely to be due to shape and size effects of the nanobelts, with increased surfaces, edges, and corners shortening the diffusion lengths of Li ions.[15] Two plateaus are evident in the first discharge process, suggesting that the lithium insertion proceeds in two steps with the first capacity ranges of 0–50 mAh g^{-1} at about 2.75 V and the second 100–175 mAh g^{-1} at about 2.30 V. We note that the lithiated MoO_3 nanobelts exhibit a discharge capacity slightly smaller than that of the non-lithiated MoO_3 nanobelts, which is likely to be due to some Li ions introduced during the secondary hydrothermal lithiation process occupying some sites that are electrochemically active for Li-storage. Figure 3B shows the curves of discharge capacity versus the cycle number for the non-lithiated and lithiated MoO_3 nanobelts at a current density of 30 mA g^{-1} and at a temperature of 25 °C. For the non-lithiated MoO_3 nanobelts, the discharge capacity decreased to 180 mAh g^{-1} after 15 cycles, corresponding to a capacity retention of 60 %. However, the discharge capacity of the lithiated MoO_3 nanobelts decreased to 220 mAh g^{-1} after 15 cycles, corresponding to a capacity retention of 92 %, showing the stability and enhanced performance of the lithiated nanobelts.

The cycling behavior can be modeled using a relation giving the capacity as a function of the cycle number, $C = C_0(1-\delta)^n$, where C_0 is the initial capacity, n is the cycle number, and δ is the fraction loss per cycle. For the non-lithiated and lithiated

ADVANCED MATERIALS

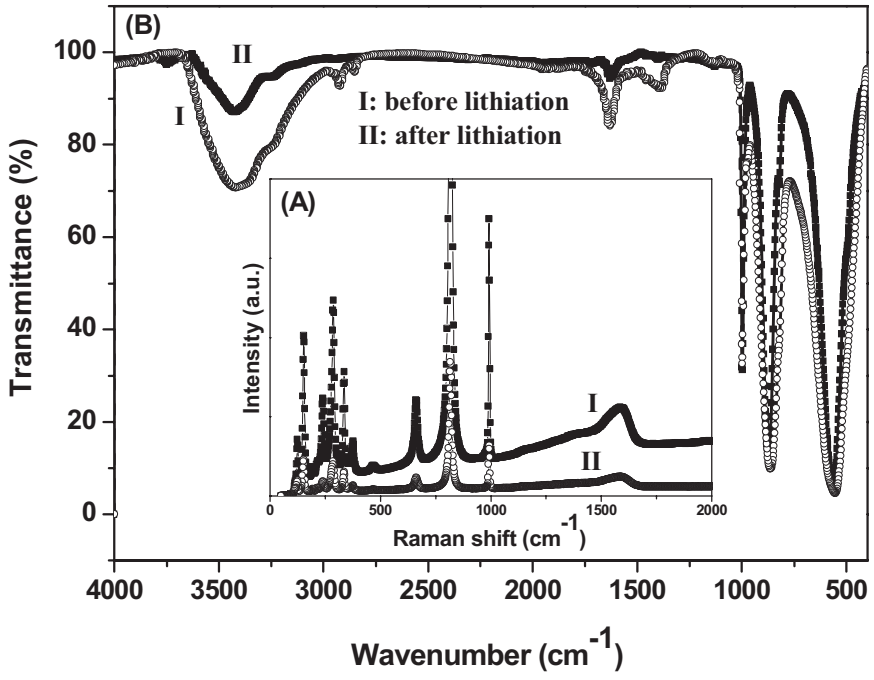

Figure 2. (A) Raman and (B) FTIR spectra of MoO_3 nanobelts before and after lithiation.

MoO_3 nanobelts, δs are 3.48 % and 0.58 %, respectively, indicating much less capacity loss per cycle for the lithiated nanobelts.

The voltage curve for the MoO_3 nanobelts exhibits an obvious hysteresis in the discharge/charge profile (Fig. 4). The hysteresis degree is determined by the difference between the potential during lithium insertion and extraction at the half reversible capacity $\Delta(V(Q/2))$. For the lithiated nanobelts, $\Delta(V(Q/2) = 0.15$ V, which is less than that of non-lithiated nanobelts ($\Delta(V(Q/2) = 0.21$ V), showing that the lithiated nanobelts exhibit better insertion/extraction reversibility.

To understand the superior performance of lithiated nanobelts for Li^+ storage, we measured the electrical transport through individual MoO_3 nanobelts before and after lithiation (Fig. 5). A single nanobelt was placed across two gold electrodes, and the final contacts were improved by Pt deposition at the two ends. Before lithiation, the *I–V* characteristics of the nanobelt showed asymmetric Schottky barriers at the two ends (the solid curve in Fig. 5), as created between semiconductor MoO_3 (with a band gap of 3.1 eV; 1 eV = 1.602×10^{-19} J) and Au/Pt electrodes, and the transported current was in the order of ca. 300 pA at ca. 2 V. After lithiation, the *I–V* curve showed ohmic behavior (the dashed curve in Fig. 5), and the transported current was of the order of 10 nA at a bias of ca. 2 V. This result suggest that the Li^+ ions introduced during lithiation effectively converted the MoO_3 nanobelts from semiconductor to metallic behavior. Using the measured resistance, the effective length, and cross section of the nanobelt, the conductivity was evaluated to be approximately 10^{-4} S cm^{-1} and 10^{-2} S cm^{-1} before and after lithiation, respectively, and therefore increased by close to two orders of magnitudes. Because the nanobelt grows along [001], the increase of conductivity along the nanobelt implies an increase of carrier density in the MoO_6 octahedral layers. This suggests that Li^+ ions have been introduced as interstitials into the layers.

Based on the voltage characteristic of the fabricated cells, the plateau of 2.75 V observed in the first discharge curve (Fig. 3A) suggests first the opening of and then the insertion into the octahedral layers of the Li^+ ions. But this plateau disappeared in the second and following discharge processes (Fig. 4A) meaning that the structure modulation was not completely reversible, resulting in less insertion of Li between the layers in later charge–discharge processes. The improvement of the cycling performance for the lithiated sample (Fig. 3B) may be attributed to the enhanced structural stability of the electrodes as a result of lithiation, which possibly indicates a reduced volumetric change of the nanobelt electrode. The Li^+ ions, first introduced during lithiation and later remaining in the lattice, enhance the electrical conductivity, which may assist the transport of the Li^+ ions to be inserted and extracted in future charge–discharge processes.

In summary, hydrothermally synthesized α-MoO_3 nanobelts were successfully lithiated by a secondary reaction with LiCl solution while retaining their crystal structure and surface morphology. The lithiated MoO_3 nanobelts exhibited excellent cycling capability, with a capacity retention rate of 92 % after 15 cycles, while the non-lithiated nanobelts retained only 60 %. Transport measurements showed that the conductivity of a lithiated MoO_3 nanobelt (10^{-2} S cm^{-1}) is increased by close to two orders of magnitudes compared to that of a non-lithiated MoO_3 nanobelt (10^{-4} S cm^{-1}), suggesting that Li^+ ions were introduced into the MoO_3 layers during lithiation. This provides a possible explanation as to why the performance of lithiated nanobelts is superior to that of non-lithiated ones. Furthermore, a secondary reaction with Li salt solution was shown to be an effective technique for improving the cycling performance and stability of MoO_3 nanobelts for applications in Li batteries.

Experimental

α-MoO_3 nanobelts were synthesized by a hydrothermal synthesis technique, and lithiation was carried out by treating the sample using LiCl. The synthesis of α-MoO_3 nanobelts was carried out as follows. $MoO_3 \cdot nH_2O$ sol was prepared by ion exchange of $(NH_4)_6Mo_7O_{24} \cdot 4H_2O$ (≥99.0 %) through a proton-exchange resin.

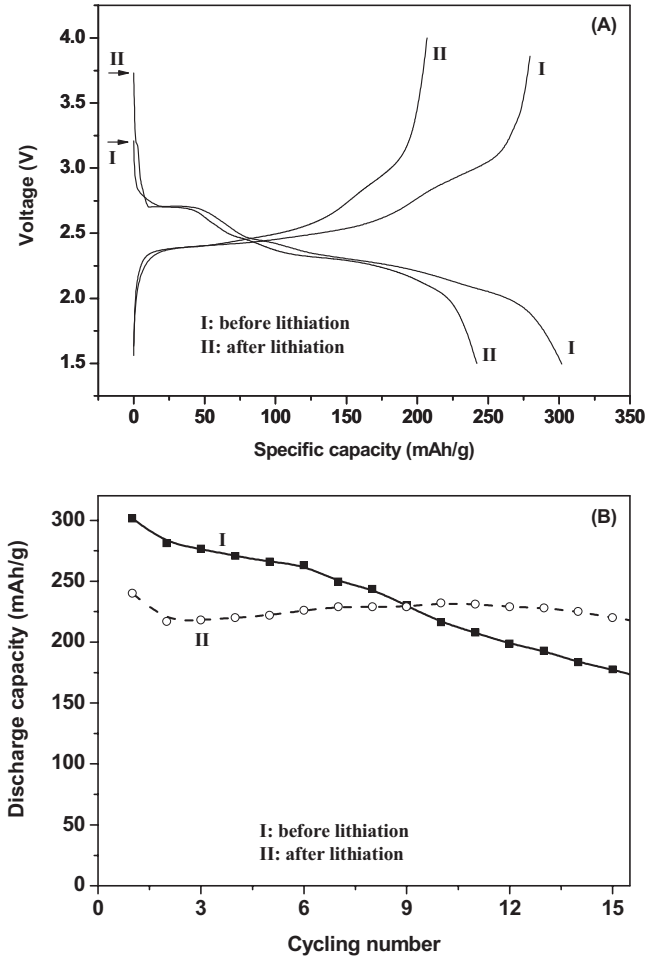

Figure 3. (A) Potential vs. capacity curves for the first cycle of charge-discharge process of the nanobelts before and after lithiation. (B) The discharge capacity as a function of the cycle number for the MoO_3 nanobelts before and after lithiation.

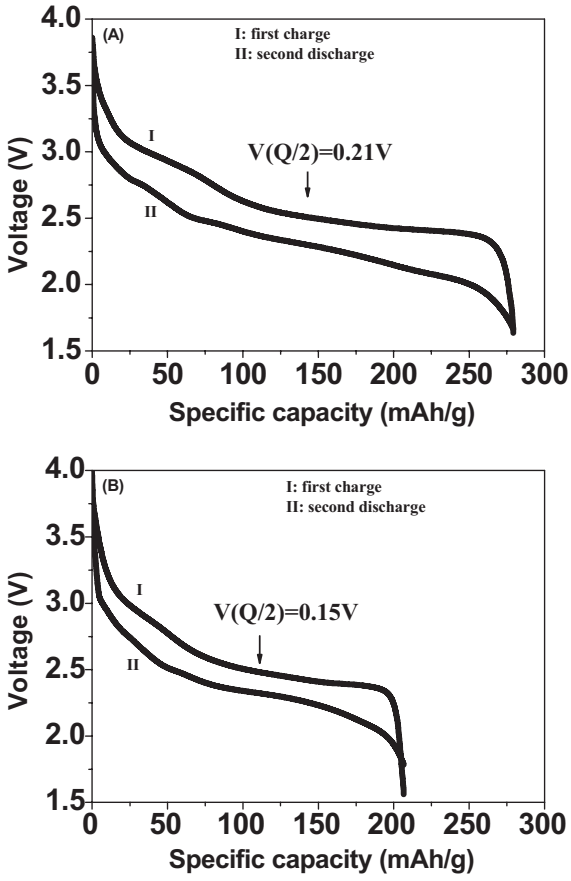

Figure 4. (A, B) Voltage hysteresis loops during the charge/discharge process for the MoO_3 nanobelts before and after lithiation, respectively.

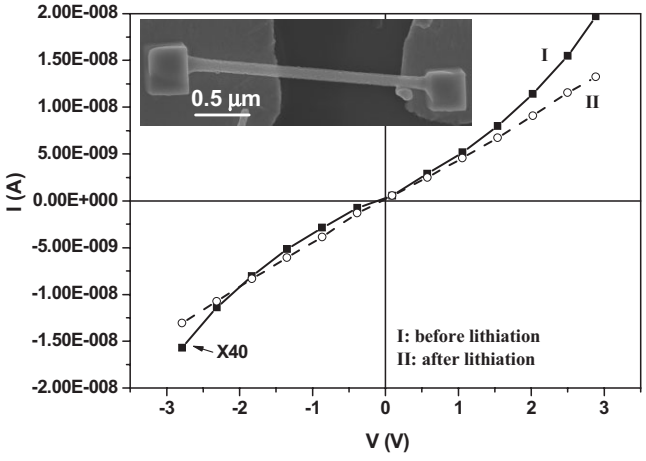

Figure 5. I-V transport measurements of single nanobelt fabricated devices using the samples before and after lithiation.

After ion exchange, a clear light-blue $MoO_3{\cdot}nH_2O$ sol (the final pH is about 2.0) was obtained. Then, the solution was directly added into a Teflon-lined autoclave and kept at 180 °C for 4 h. After the hydrothermal reaction, the light-blue product was washed with distilled water and ethanol and then dried at 80 °C for 8 h. To attain the lithiated MoO_3 nanobelts, 0.20 g MoO_3 nanobelts were dispersed by ultrasonic treatment in deionized water for half an hour. Subsequently the dispersed MoO_3 nanobelts were stirred with 0.29 g LiCl for 2 days, and the resultant light-blue solution was transferred to a 50 mL Teflon-lined autoclave. The autoclave was sealed and heated at 180 °C for 24 h. Next, the autoclave was left to cool down in air and the solid precipitate was filtered out and washed with deionized water at least five times to remove the LiCl adsorbed on the surface of the nanobelts. The resulting "slurry" was allowed to dry on the filter paper at 100 °C.

Received: April 13, 2007
Revised: August 2, 2007

[1] J. Maier, *Nat. Mater.* **2005**, *4*, 805.
[2] Y. S. Hu, L. Kienle, Y. G. Guo, J. Maier, *Adv. Mater.* **2006**, *18*, 1421.
[3] L. Q. Mai, W. Chen, Q. Xu, J. F. Peng, Q. Y. Zhu, *Chem. Phys. Lett.* **2003**, *382*, 307.
[4] X. W. Lou, H. C. Zeng, *Chem. Mater.* **2002**, *14*, 4781.
[5] L. Q. Mai, W. Chen, Q. Xu, Q. Y. Zhu, *Microelectron. Eng.* **2003**, *66*, 199.
[6] J. Zhou, N. S. Xu, S. Z. Deng, J. Chen, J. C. She, Z. L. Wang, *Adv. Mater.* **2003**, *15*, 1835.

[7] X. L. Li, J. F. Liu, Y. D. Li, *Appl. Phys. Lett.* **2002**, *81*, 4832.
[8] J. B. Sun, R. Xiong, S. M. Wang, W. F. Tang, H. Tong, J. Shi, *J. Sol-Gel Sci. Tech.* **2003**, *27*, 315.
[9] I. J. Ramirez, A. Martinez-de la Cruz, *J. Solid State Electrochem.* **2003**, *7*, 259.
[10] L. Q. Mai, C. S. Lao, B. Hu, J. Zhou, Y. Y. Qi, W. Chen, E. D. Gu, Z. L. Wang, *J. Phys. Chem. B* **2006**, *110*, 18 138.
[11] S. T. Wang, Y. G. Zhang, X. C. Ma, W. Z. Wang, X. B. Li, Z. D. Zhang, Y. T. Qian, *Solid State Commun.* **2005**, *136*, 283.
[12] G. A. Nazri, C. Julien, *Solid State Ionics* **1992**, *53-6*, 376.
[13] G. Guzman, B. Yebka, J. Livage, C. Julien, *Solid State Ionics* **1996**, *86-8*, 407.
[14] W. Dong, B. Dunn, *J. Non-Cryst. Solids* **1998**, *225*, 135.
[15] Z. H. Wen, Q. Wang, J. H. Li, *J. Nanosci. Nanotechnol.* **2006**, *6*, 2117.

